

# Dye-doped organic distributed-feedback lasers with index and surface gratings: the role of pump polarization and molecular orientation

Daniel Wright, Etienne Brasselet, and Joseph Zyss

*Laboratoire de Photonique Quantique et Moléculaire, Ecole Normale Supérieure de Cachan, 61 avenue du Président Wilson, 94235 Cachan, France*

Gregor Langer and Wolfgang Kern

*Institut für Chemische Technologie organischer Stoffe, Technical University of Graz, Stremayrgasse 16, 8010 Graz, Austria*

Manuscript received September 16, 2003; revised manuscript received December 5, 2003; accepted January 20, 2004

The dependence of the laser threshold of organic distributed-feedback (DFB) lasers having index and surface gratings on the pump polarization angle is studied and examined. A model is developed to describe the relationship between the fluorophore orientational distribution and the number of photons emitted into the laser mode. Experimental data fitted with this model demonstrate that the fluorophores are isotropically oriented in the plane of the sample. The polarization dependence of the laser threshold is then used in conjunction with the measured pump intensity dependence of the emission intensity to explain the pump polarization selectivity of the laser emission of these structures. The effect of the above phenomena on future applications is discussed. © 2004 Optical Society of America

OCIS codes: 140.3490, 250.3680, 160.3380, 160.4890.

## 1. INTRODUCTION

The study and development of organic thin-film lasers has been of interest to many researchers because of their potential for telecommunications applications. During the 1990s this research domain was greatly motivated and assisted by the considerable progress of organic light-emitting diodes<sup>1</sup> because the materials employed are similar for these related devices. Organic materials are attractive for many applications because of their ability to form lightweight and low-cost device structures through use of relatively simple preparation methods such as photolithography,<sup>2,3</sup> ink-jet printing,<sup>4,5</sup> and micromolding<sup>6,7</sup> on a variety of substrates including curved<sup>8</sup> and flexible<sup>7</sup> ones. In addition to these advantages, organic materials have several properties that are especially interesting for laser applications. The large Stokes shift between absorption and emission reduces self-absorption losses, thereby increasing the net gain and lowering the laser threshold. This separation between absorption and emission can be further augmented by use of fluorescence resonance energy-transfer fluorophore pairs.<sup>9</sup> In addition, fundamental laser characteristics such as the output wavelength and the laser threshold have a much weaker temperature dependence than their inorganic counterparts, thus easing the requirements of external temperature stabilizing.<sup>10,11</sup> One of the major remaining challenges is to create organic lasers that can be pumped electrically; thus far, to our knowledge, all the lasers based on amorphous organic materials presented in the literature have been optically pumped. Despite this limi-

tation, applications are still possible within the regime of optical pumping; devices in which an organic laser is pumped by a low-cost microchip laser have recently been proposed and demonstrated.<sup>2,3,12,13</sup>

Organic thin-film lasers can be fabricated from a variety of materials including spin-cast polymers, evaporated molecules, or liquid-crystal matrices<sup>14</sup> that are subsequently sculpted into various resonator structures.<sup>1,15,16</sup> One of the more widely used and robust resonators is the distributed-feedback (DFB) type because these lasers are relatively easy to fabricate and they provide good laser performance. In this class of lasers, the grating period ( $\Lambda$ ) of the periodic index or gain pattern determines the emission wavelength that can be written as  $\lambda_L = 2\Lambda n_{\text{eff}}/m$  where  $n_{\text{eff}}$  is the effective refractive index of the guided mode and  $m$  is the order of diffraction responsible for the feedback. This property allows simple determination of the emission wavelength during sample fabrication or during laser operation when transient gratings are used.<sup>13</sup> The tuning range is limited only by the gain spectrum of the fluorophore or fluorescing polymer used, which can be upwards of 100 nm. This range can be shifted by use of different dye molecules or emitting polymers, which enables organic DFB laser operation from  $\sim 450$  to 1000 nm.<sup>9,17</sup> DFB lasers with index gratings provide an additional advantage in that the order of the grating can be used to control the direction of the light output. A DFB laser that uses first-order diffraction for feedback will emit only at each end of the grating, analogous to standard two-mirror lasers. Lasers that use

higher orders of diffraction will have a fraction of the light diffracted in other directions as well, depending on the order used.<sup>18</sup> For most applications, first- or second-order diffraction is used, with second-order diffraction being attractive because light is emitted perpendicular to the surface. Two-dimensional (2-D) structures such as the superposition of two perpendicular sign waves<sup>3</sup> or circular gratings<sup>19</sup> can be employed to achieve a collimated beam perpendicular to the sample surface.

Although many organic DFB lasers composed of a host of different organic materials have been described in the literature, thus far, to our knowledge, the role of the pump beam polarization on the laser properties has yet to be fully examined. In this paper we study the modification of the laser characteristics induced when the incoming polarization is rotated and propose optimization techniques for dye-doped organic DFB lasers having simple index gratings as well as those having index gratings superimposed with surface-relief and surface ablation gratings.

## 2. MATERIALS

### A. Photopolymer Poly(styrene-co-4-vinylbenzyl thiocyanate)

The samples studied in this research were optically patterned structures of poly(styrene-co-4-vinylbenzyl thiocyanate) (PST-co-VBT), which is a photopolymer material amenable to deep-UV recording at  $\lambda < 290$  nm. The underlying mechanism that results in a change of the refractive index and a change of the film thickness is based on an UV photoisomerization process involving the transformation of the thiocyanate group (SCN) into an isothiocyanate group (NCS). The NCS moiety can be further modified with reactive gas-phase chemical treatment that results in an additional index change accompanied by the formation of a surface-relief grating.<sup>20,21</sup> In recent studies second-order DFB lasing has been demonstrated in 4-dicyanmethylene-2-methyl-6-4H-pyran- (DCM-) doped PST-co-VBT films patterned by holographically inscribed index and surface-relief gratings, where one-dimensional<sup>22,23</sup> and 2-D<sup>24</sup> gratings provided the resonator systems for organic surface-emitting laser devices in the visible.

PST-co-VBT was synthesized according to a published procedure<sup>20</sup> and codissolved with DCM (Radiant Dyes, 2 wt. %) in  $\text{CHCl}_3$ . The resulting solutions were filtered (0.2- $\mu\text{m}$  pore size) and subsequently spun onto  $\text{CaF}_2$  substrates (Suss RC5 spin coater). The thickness and refractive index of the films were measured by spectroscopic ellipsometry (Woollam variable angle of incidence spectroscopic ellipsometer).

### B. Interference Lithography

Interferometric patterning was carried out with the fourth harmonic of a 10-Hz Nd:YAG laser (Spectra Physik/Quanta Ray-GCR 170-10) at  $\lambda = 266$  nm. Pulse energies were determined with a pyroelectric joulemeter (Gentec ED-200). The laser beam (diameter  $\sim 7$  mm) was split in two with a beam splitter (Laser Components BS266/45 S50) and then recombined on the sample plane at an angle  $\theta$  to produce a periodic fringing pattern. By

changing the incident angle  $\theta$  of the laser beams interfering at the sample surface, we could adjust the grating period  $\Lambda$  according to the relation  $\Lambda = \lambda/2 \sin \theta$ , where  $\lambda$  is the irradiation wavelength and  $\theta$  is the incident angle of the writing beams. Irradiations of 40 pulses with a total energy density of  $\sim 6 \text{ mJ cm}^{-2}$  per pulse resulted in a refractive-index pattern, whereas higher-energy densities ( $> 14 \text{ mJ cm}^{-2}$  per pulse) led to laser ablation-induced surface gratings in addition to the refractive-index pattern.<sup>22,23</sup> All interference illuminations were carried out in an ambient atmosphere.

### C. Postexposure Modification of PST-co-VBT Films

We carried out conversion of photogenerated NCS groups to thiourea units by placing the polymer samples over solutions of propylamine and ethylenediamine (propylamine, 2.5 wt. % in toluene; ethylenediamine, 1.0 wt. % in toluene). The modification reactions were carried out at 20 °C for 120 s. For reactions with ammonia, the illuminated polymer films were placed in an IR cell (Graseby-Specac) thermostated at 50 °C, which was filled with gaseous ammonia (reaction time 60 min). Hydrazine hydrate (Aldrich) was dehydrated with solid potassium hydroxide following a literature method and placed in a thermostatically controlled vessel (70 °C). Vapors of hydrazine carried in a stream of dry nitrogen were passed through a reaction chamber containing the polymer sample at 20 °C (reaction time 30 s). After the postexposure modification, the samples were stored in vacuum to remove excess reagents.

The depth and grating period of the resulting surface gratings produced by gas modification and laser ablation were measured by atomic force microscopy (Nano Scope IIIa and Dimension 3100, Digital Instruments) in tapping mode. Film thicknesses were measured by spectrometric ellipsometry with an error of  $\sim 5\%$ .

## 3. DISTRIBUTED-FEEDBACK LASER CHARACTERISTICS

We studied the DFB lasers for this research using the experimental setup shown in Fig. 1. Laser light from a doubled Nd:YAG laser that provided  $\sim 20$ -ps pulses at 10 Hz and 532 nm was focused to a spot of radius in the range of 600–800  $\mu\text{m}$  (measured with a knife blade technique) on the DFB samples at normal incidence. A pass-band filter was placed before the sample to eliminate light from the flash lamps and other harmonics of the pump laser. A half-wave plate placed in front of a polarizer was used to control the pump power on the sample while a sec-

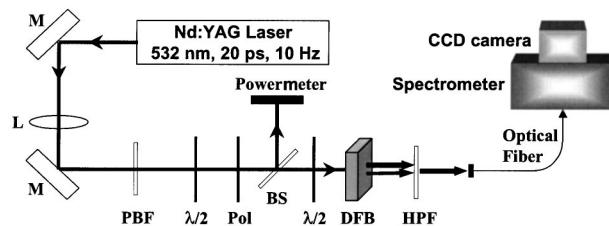


Fig. 1. Experimental apparatus. M, mirror; L, lens; PBF, pass-band filter; Pol, polarizer; BS, beam splitter;  $\lambda/2$ , half-wave plate; HPF, high-pass filter.

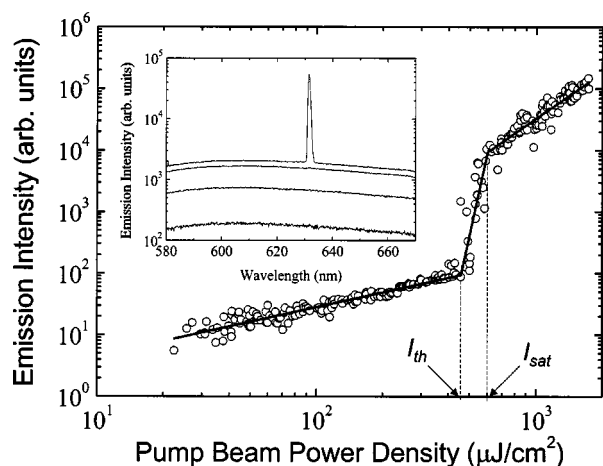


Fig. 2. Typical plot of the laser emission intensity versus the pump power density for a DFB laser sample. The curves are power-law fits. The input-output behavior is characterized by a fluorescence region ( $I_{\text{pump}} < I_{\text{th}}$ ), the onset point ( $I_{\text{th}}$ ), the transition region ( $I_{\text{th}} < I_{\text{pump}} < I_{\text{sat}}$ ), the saturation point ( $I_{\text{sat}}$ ), and the saturation region ( $I_{\text{pump}} > I_{\text{sat}}$ ). Inset: Several emission spectra obtained with increasing pump power. At low intensities a broad fluorescence background is observed; above the laser threshold a narrow peak emerges.

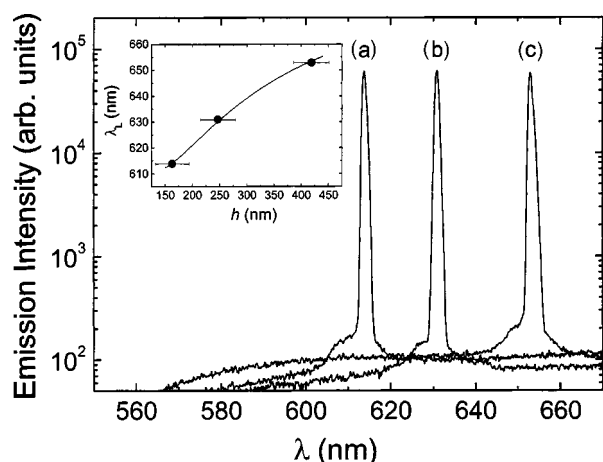


Fig. 3. Saturated laser emission spectra for DFB samples of various thicknesses: (a) 163 nm, (b) 247 nm, (c) 419 nm. Inset: Peak emission wavelength versus film thickness. The solid-curve fit is described in the text.

ond half-wave plate placed just before the sample was used to control the incident pump polarization angle. A glass plate was used to divert several percent of the pump beam to a powermeter that was used as a reference of the pump beam power. After the sample, a high-pass filter removed the transmitted pump light. Laser light emitted from the surface of the DFB laser was subsequently collected by a fiber bundle of  $\sim 1$  mm in diameter. This light was then coupled into a spectrograph (Model MS125, Oriel Instruments), which dispersed the emission onto the pixels of a cooled CCD camera (Andor Technologies). The spectrometer was calibrated with the 532-nm line of the pump laser.

We performed the laser threshold measurements by obtaining 300 single-shot emission spectra for a given sample at different pump intensities  $I_{\text{pump}}$ . Several examples of such one-shot spectra at different intensities

are presented in the inset of Fig. 2. The area under the laser peak was then integrated for all spectra; typical results of this measurement are plotted in Fig. 2. We can clearly see three regimes; for  $I_{\text{pump}} < I_{\text{th}}$  a nearly linear regime is visible that is indicative of fluorescence, which is followed by a steep transition to laser action at  $I_{\text{th}} < I_{\text{pump}} < I_{\text{sat}}$ , and finally a saturation region where  $I_{\text{pump}} > I_{\text{sat}}$ .

In this study experiments were carried out on DFB lasers of different thicknesses (namely, 163, 247, and 419 nm) to investigate any effect on the observed phenomena. The saturated emission spectra of the resulting devices were recorded for each device, the results of which are shown in Fig. 3. For each sample thickness we observe similar characteristics, with each spectrum consisting of a single laser emission peak that is several orders of magnitude more intense than the fluorescence background. The emission displays an instrument-limited spectral linewidth of  $\sim 1$  nm and is polarized parallel to the grating lines of the sample with a ratio of  $>250:1$ , regardless of the pump polarization. The laser emission wavelength  $\lambda_L$  of each sample thickness is plotted in the inset of Fig. 3. The observed behavior can be understood when the samples are modeled as asymmetric planar waveguides.<sup>12,18</sup> The best fit to the data is shown in the inset of Fig. 3, which gives a grating period of 426 nm and a bulk index of refraction of 1.607, which are in good agreement with the values of 430 nm and 1.613 measured by atomic force microscopy and ellipsometry, respectively.

#### 4. POLARIZATION EFFECTS AND DYE ORIENTATION

In this section we describe the influence of the fluorophore orientational distribution in the polymeric film  $f(\Omega)$  (where  $\Omega$  represents the three-dimensional (3-D) dipole orientation angles) on the DFB laser characteristics, specifically the pump angle dependence of the laser threshold. Because the laser oscillation occurs in the direction of the grating wave vector  $\mathbf{K}$  [see Fig. 4(a)], it is expected that both the distribution  $f(\Omega)$  and the polarization direction  $\mathbf{e} = (\cos \alpha, \sin \alpha, 0)$  of the excitation electric field  $\mathbf{E} = E_0 \mathbf{e}$  (Fig. 5) are of paramount importance for the laser threshold and pump polarization selectivity. We present

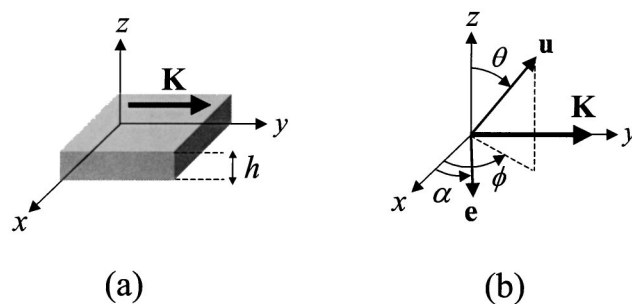


Fig. 4. General DFB sample characteristics. (a) Diagram of the sample structure with  $h$  the thickness and  $\mathbf{K}$  the grating wave vector of the grating. Coordinate systems used for the chromophore orientational distributions, with  $\mathbf{u}$  the vector representing the fluorophore dipole and  $\mathbf{e}$  the unit vector representing the polarization direction of the linearly polarized pumping beam.

a formalism that allows the determination of the pump angle dependence of  $I_{\text{th}}$ . The model is developed through examination of the fluorescence intensity along the DFB grating wave vector  $\mathbf{K}$  (which lies along the  $y$  direction),  $I_y$ , which is evaluated as

$$I_y \propto \int_{\Omega} P_{\text{abs.}}(\Omega) \Pi_y(\Omega) f(\Omega) d\Omega, \quad (1)$$

where  $P_{\text{abs.}} \propto |\mathbf{E} \cdot \boldsymbol{\mu}|^2$  is the absorption probability of the dye molecules with  $\boldsymbol{\mu} = \mu \mathbf{u}$  the fluorophore excitation transition dipole,  $\mathbf{u}$  a unit vector along the vector dipole axis,  $\Pi_y$  the Poynting vector in the  $y$  direction, and  $f(\Omega)$  the orientational distribution of the laser dye molecules in the organic thin film. Assuming unidimensional fluorophores characterized by the unit vector  $\mathbf{u} = (\sin \theta \cos \phi, \sin \theta \sin \phi, \cos \theta)$  where  $\theta$  and  $\phi$  are the dipole orientation angles [Fig. 4(b)] and using the far-field approximation for the dipole radiation, we obtain

$$P_{\text{abs.}} \propto (\mathbf{e} \cdot \mathbf{u})^2 = (\cos^2 \alpha \cos^2 \phi + \sin^2 \alpha \sin^2 \phi) \sin^2 \theta, \quad (2a)$$

$$\Pi_y \propto (\mathbf{y} \times \mathbf{u})^2 = \cos^2 \theta + \sin^2 \theta \cos^2 \phi. \quad (2b)$$

In the general case we obtain

$$I_y(\alpha) \propto \int_0^{2\pi} d\phi \int_0^{\pi} f(\theta, \phi) (\cos^2 \alpha \cos 2\phi + \sin^2 \phi) \times (\cos^2 \theta + \sin^2 \theta \cos^2 \phi) \sin^3 \theta d\theta. \quad (3)$$

At this point, knowledge of the distribution  $f(\theta, \phi)$  is required. From Fig. 5, which shows that the fluorescence intensity is independent of the pump polarization direction  $\alpha$ , we deduce that the dye distribution is invariant by rotation around the  $z$  axis. For the sake of simplicity we assume the following generic normalized distribution that satisfies this symmetry argument:

$$f(\theta, \phi) = f_0 \quad \text{if } \pi/2 - \beta \leq \theta \leq \pi/2 + \beta, \quad 0 \leq \phi \leq 2\pi, \\ f(\theta, \phi) = 0 \quad \text{otherwise}, \quad (4)$$

where  $f_0 = 1/(4\pi \sin \beta)$  is a normalization constant and  $\beta$  is an angle that characterizes the extent of orientation out of the sample plane ( $x, y$ ). The distribution employed is admittedly not physical, but serves as a first approximation to a real distribution. Integration over space yields

$$I_y(\alpha, \beta) \propto F(\beta) + G(\beta) \cos^2 \alpha, \quad (5)$$

where

$$F(\beta) = 16 + 8 \cos^2 \beta - 9 \cos^4 \beta, \\ G(\beta) = 16 + 8 \cos^2 \beta + 6 \cos^4 \beta. \quad (6)$$

Because the laser threshold intensity  $I_{\text{th}}(\alpha)$  corresponds to a given amount of fluorescence intensity along  $\mathbf{K}$ , we finally obtain

$$I_{\text{th}}(\alpha, \beta) = \frac{F(\beta) + G(\beta)}{F(\beta) + G(\beta) \cos^2 \alpha} I_{\text{th}}(0). \quad (7)$$

Equation (7) predicts that the laser threshold  $I_{\text{th}}$  is a  $\pi$ -periodic function of the pump polarization direction  $\alpha$ ,

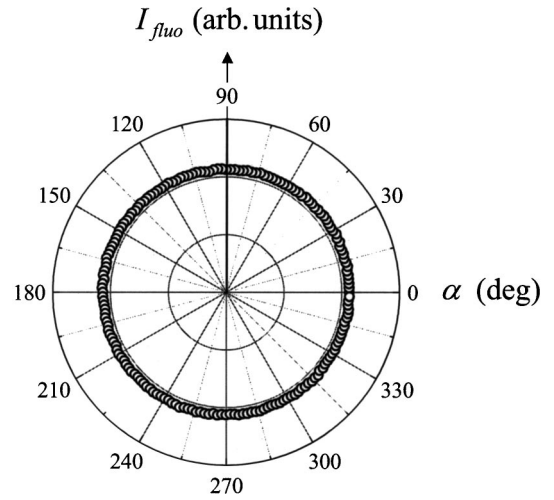


Fig. 5. Dependence of the fluorescence emission with respect to the pump polarization angle  $\alpha$  for a DFB sample thickness of 419 nm.

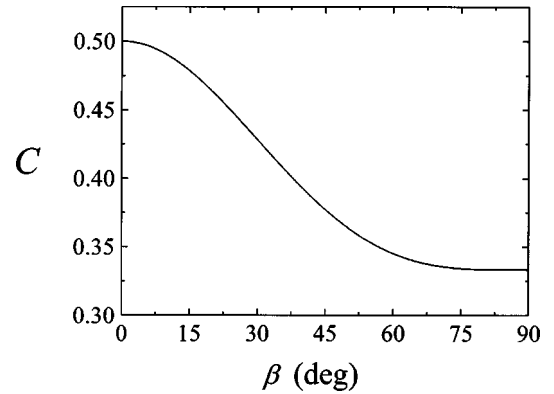


Fig. 6. Contrast  $C$  of Eq. (8) plotted versus angle  $\beta$ .

with the maxima located at  $\alpha = (n + 1/2)\pi$  and the minima at  $\alpha = n\pi$ , where  $n$  is an integer. The contrast of the oscillating function  $I_{\text{th}}(\alpha)$ , defined by  $C = (I_{\text{th}}^{\text{max}} - I_{\text{th}}^{\text{min}})/(I_{\text{th}}^{\text{max}} + I_{\text{th}}^{\text{min}})$ , is a function of the angle  $\beta$ . From Eq. (7) we find

$$C(\beta) = \frac{G(\beta)}{2F(\beta) + G(\beta)}, \quad (8)$$

which is plotted in Fig. 6. From Fig. 6 we can foresee that the measurement of  $C$  could allow the determination of the angle  $\beta$ . However, one must keep in mind that values obtained near  $\beta = 0^\circ$  and  $90^\circ$  will only be qualitative because the relative variations of the contrast are small in these ranges. Figure 7 presents the measured laser threshold as a function of the pump beam polarization direction (circles) for a sample thickness of  $h = 419$  nm. The threshold is at a maximum when the pump laser polarization is polarized perpendicular to the grating lines ( $\alpha = 90^\circ$  and  $270^\circ$ ) because most of the emitted radiation is radiated perpendicularly to the grating direction, whereas it is minimized when the polarization is parallel to the grating lines ( $\alpha = 0^\circ$  and  $180^\circ$ ). We note that this efficiency maximum is valid for a normal-incidence pump-geometry.

The solid curve corresponds to the best fit by use of Eq. (7), which yields  $\beta = 0^\circ$  (in-plane isotropic dye distribution) and is in agreement with the data. This fit contained an extra factor of  $\exp(-\alpha/\alpha_c)$  to phenomenologically take into account the dye degradation (or bleaching) that occurs during the experiment. The fit in Fig. 7 yielded an  $\alpha_c$  of  $800^\circ$ . This angle relates to the increase in threshold that is induced with each measurement. As described above, each point in Fig. 7 corresponds to 300 one-shot spectra that are obtained for a range of intensities that varied only weakly with the pump polarization angle. The resulting fluence absorbed by the sample for each measurement point is roughly 30 mJ.

These results suggest that an orientational effect is the origin of the observed behavior. The origin of the 2-D distribution found by the fits can be found in the fact that spin-coated thin polymeric films (a few hundreds of nanometers) have their chains aligned principally parallel to the substrate plane, which in turn may force the dye molecules to also be in plane because of guest–host molecular interactions. We repeated these experiments for the various samples of different thicknesses mentioned above (163, 246, and 419 nm) as well as for samples that have index gratings superimposed with surface-relief and surface ablation gratings and arrived at the same conclusions in all cases. To further confirm our interpretation, we attempted to alter the initial fluorophore distribution by heating samples for 24 h at  $120^\circ\text{C}$  (sample  $T_g \approx 100^\circ\text{C}$ ). Heating the sample should randomize the fluorophore distribution, leading to a larger  $\beta$  and reduced contrast  $C$  in the above analysis. After heating,  $\beta = 17^\circ$  was found, which corresponds to a partial randomization of the fluorophore distribution. As an aside, the maximum relative variation of the laser threshold due to heating was 3%, demonstrating the good thermal stability of the laser properties in these films.

To illustrate the difference between the observed behavior and that expected for a three-dimensionally isotropic dye distribution ( $\beta = 90^\circ$ ), Fig. 7 also displays the corresponding laser threshold dependence in this case (see dashed curve), which emphasizes the importance of

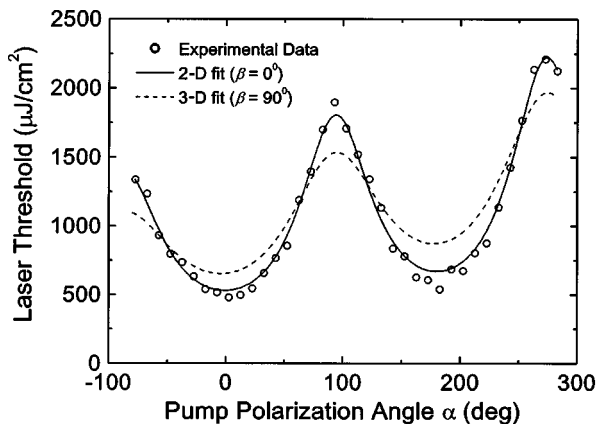


Fig. 7. Dependence of the laser threshold on the angle of polarization  $\alpha$  for a DFB sample thickness of 419 nm. The dashed-curve fit assumes a 3-D isotropic chromophore orientational distribution, whereas the solid curve assumes that the chromophores are isotropically distributed in the  $(x, y)$  sample plane.

both the fluorophore distribution and the operating conditions to obtain the lowest laser thresholds. Optimization of both the absorption probability and the dipole radiation along the  $y$  direction are required, as can be seen from relations (1) and (2). With this in mind it is possible to foresee applications based on the manipulation of the dye orientational distribution, which could be achieved by thermal poling, photoassisted thermal poling, or all-optical poling techniques.<sup>25</sup> For example, we can lower the threshold by orientating the dye molecules parallel to the  $x$  direction. On the other hand, if these lasers are pumped by poorly or unpolarized sources (such as diode lasers or lasers coupled with non-polarization-preserving fibers), a lasing intensity insensitive to the pump polarization is required. From Fig. 7 it is clear that the dye distribution resulting from normal DFB laser fabrication (Section 2) does not meet such requirements. However, a judicious manipulation of the orientational distribution should lead to a polarization-independent lasing intensity.

The pump polarization angle dependence of the DFB laser properties will be particularly important when samples are used that have several multiplexed gratings. In this case the isotropic 2-D dye distribution is the most suitable to obtain equal performance for each superimposed laser. Pump polarization selectivity and prospectives for samples incorporating multiple DFB gratings are discussed in Section 5.

## 5. PUMP POLARIZATION SELECTIVITY

We examined the pump polarization angle dependence of the emission intensity by varying the pump polarization angle ( $\alpha$ ) while keeping the excitation intensity  $I_0$  fixed. The filled circles in Figs. 8(a) and 8(b) show the results for two different input intensities above the laser threshold. It is clear from Figs. 8(a) and 8(b) that the pump polarization selectivity is increased when the pump intensity is close to the laser threshold. In addition, angular thresholds can be observed as kinks in the angular emission pattern [Figs. 8(a) and 8(b)], with  $\alpha_{\text{th}}$  and  $\alpha_{\text{sat}}$  the angular analogs of the intensity thresholds  $I_{\text{th}}$  and  $I_{\text{sat}}$  (Fig. 2). This can be well understood on the basis of the results of Section 4. We use the laser threshold dependence versus the pump polarization angle  $\alpha$  that is deduced from Eqs. (6) and (7) and the condition  $\beta = 0^\circ$  (2-D distribution) to find the pump polarization angle dependence of the laser threshold:

$$I_{\text{th}}^{2\text{-D}}(\alpha) = g(\alpha)I_{\text{th}}^{2\text{-D}}(0), \quad (9)$$

where

$$g(\alpha) = \frac{3}{1 + 2 \cos^2 \alpha}. \quad (10)$$

On the basis of the results of Section 3, we assume a multilinear input–output curve in  $\log I_{\text{pump}}$  versus  $\log I_L$  representation, where  $I_{\text{pump}}$  is the pump beam intensity and  $I_L$  is the emitted intensity (see Fig. 2) of the form

$$\log I_L = a_1 \log I_{\text{pump}} + b_1 \quad \text{if } I_{\text{pump}} \leq I_{\text{th}}^{2\text{-D}}(\alpha),$$

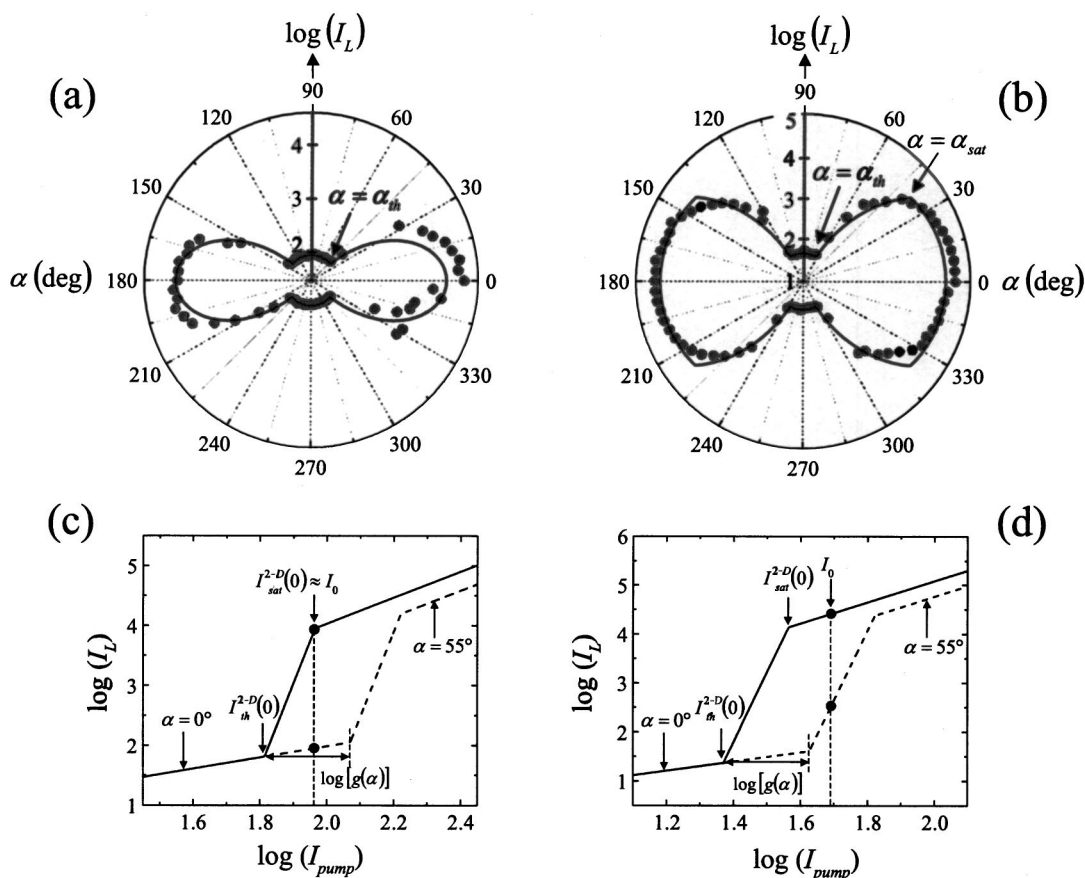


Fig. 8. Pump angle dependence of the emitted intensity in the spectral window of the laser peak at two different pump power densities (a)  $\sim 1.4$  and (b)  $\sim 2.8$  times the laser threshold and their corresponding representation (c) input and (d) output curves. The solid and dashed lines in (c) and (d) represent the corresponding curves for  $\alpha = 0^\circ$  and  $55^\circ$ , respectively. The fits in (a) and (b) are described in the text.

$$\log I_L = a_2 \log I_{\text{pump}} + b_2$$

$$\text{if } I_{\text{th}}^{2-D}(\alpha) \leq I_{\text{pump}} \leq I_{\text{sat}}^{2-D}(\alpha),$$

$$\log I_L = a_3 \log I_{\text{pump}} + b_3 \quad \text{if } I_{\text{sat}}^{2-D}(\alpha) \leq I_{\text{pump}}, \quad (11)$$

where the different slopes  $a_i$  are constants for a given sample. For the laser that corresponds to the data of Figs. 8(a) and 8(b), the experimental averaged values over ten independent measurements are, respectively,  $a_1 = 0.94 \pm 0.03$ ,  $a_2 = 14.2 \pm 3.3$ , and  $a_3 = 2.17 \pm 0.25$ . Finally, we fitted the experimental angular spectra using the coefficients  $b_i$  as adjustable parameters from which we deduce  $I_{\text{th}}^{2-D}(0)$ ,  $I_{\text{sat}}^{2-D}(0)$ , and  $I_0$  from Eqs. (9)–(11). The best fits are denoted by the solid curves in Figs. 8(a) and 8(b). Figures 8(c) and 8(d) present the corresponding behavior in the  $(\log I_{\text{pump}}, \log I_L)$  representation for  $\alpha = 0^\circ$  (solid lines) and  $\alpha = 55^\circ$  (dashed lines). Increasing the pumping polarization angle has the effect of shifting the entire input–output curve to higher pumping intensities. Good agreement with the experimental data is found, and we conclude that it is preferable to work below the saturation regime to reach high pump polarization selectivity.

The main source of disagreement between the fit and the experimental data is the same fluorophore degradation process observed in Fig. 7, which is not accounted for

in the fitting procedure. The effects of degradation are even clearer in these experiments because the emission intensity is nonlinearly dependent on the number of active molecules. The effect is visible as a discontinuity and a lack of symmetry about the experimental starting point of  $0^\circ$ . Although dye degradation limits the applicability of these materials to marketable devices, it should be noted that all experiments in this study were carried out in ambient conditions and no efforts were made to improve this aspect of the sample performance.

In light of these results on pump polarization selectivity, we can foresee a multiple DFB laser obtained from the superimposition of different gratings with noncollinear wave vectors. Such multiplexed DFB laser structures have been recently realized and are discussed in a separate paper.<sup>26</sup>

## 6. CONCLUSION

In this paper we have examined the effect of pump beam polarization on the laser threshold and emission intensity in optically pumped dye-doped organic DFB lasers. DCM-doped PST-co-VBT samples having refractive-index gratings formed from periodic UV illumination were used as model systems. Sample fluorescence spectra were observed to be independent of the pump polarization angle, suggesting that the 3-D fluorophore distribution is isotro-

pic in the sample plane. A theoretical model that links the fluorophore orientation distribution in the sample to the laser threshold was then developed and used to fit experimental data from experiments in which the laser threshold was measured with respect to the pump polarization angle. Resulting fits showed that the fluorophores lie predominantly in the sample plane with no preferred direction. These results were shown to be general for thin-film samples with thicknesses of several hundred nanometers and grating types (simple index gratings, index gratings superimposed with surface-relief or surface ablation gratings). The pump angle dependence of the laser threshold was then combined with the measured input-output characteristics of the DFB lasers to explain the dependence of the emission intensity on the pump polarization angle, which has strong implications on the pump polarization selectivity of the resonators. The analysis presented here underlines the importance of pump polarization selectivity in applications that employ organic DFB lasers because the pump polarization selectivity needs to be properly tuned to maximize performance. The optimization of the fluorophore distribution for different applications will be the subject of future research.

## ACKNOWLEDGMENTS

The authors thank K. F. Iskra and T. Neger for holographic patterning, G. Jakopic (Joanneum Research, Austria) for ellipsometric measurements, and A. Pogantsch for helpful discussions. D. Wright acknowledges the National Science Foundation for the International Research Postdoctoral Fellowship. W. Kern and G. Langer acknowledge financial support by Spezialforschungsbereich Elektroaktive Stoffe (Technical University of Graz) and Fonds zur Förderung der wissenschaftlichen Forschung (Vienna) within project 921.

## REFERENCES

1. M. D. McGehee and A. J. Heeger, "Semiconducting (conjugated) polymers as materials for solid-state lasers," *Adv. Mater.* **12**, 1655–1668 (2000).
2. Y. Oki, S. Miyamoto, M. Maeda, and N. J. Vasa, "Multi-wavelength distributed-feedback dye laser array and its application to spectroscopy," *Opt. Lett.* **27**, 1220–1222 (2002).
3. G. A. Turnbull, P. Andrew, W. L. Barnes, and I. D. W. Samuel, "Operating characteristics of a semiconducting polymer laser pumped by a microchip laser," *Appl. Phys. Lett.* **82**, 313–315 (2003).
4. T. R. Hebner, C. C. Wu, D. Marcy, M. H. Lu, and J. C. Sturm, "Ink-jet printing of doped polymers for organic light emitting devices," *Appl. Phys. Lett.* **72**, 519–521 (1998).
5. S. C. Chang, J. Liu, J. Bharathan, Y. Yang, J. Onohara, and J. Kido, "Multicolor organic light-emitting diodes processed by hybrid inkjet printing," *Adv. Mater.* **11**, 734–737 (1999).
6. J. R. Lawrence, P. Andrew, W. L. Barnes, M. Buck, G. A. Turnbull, and I. D. W. Samuel, "Optical properties of a light-emitting polymer directly patterned by soft lithography," *Appl. Phys. Lett.* **81**, 1955–1957 (2002).
7. M. Berggren, A. Dodabalapur, R. E. Slusher, A. Timko, and O. Nalamasu, "Organic solid-state lasers with imprinted gratings on plastic substrates," *Appl. Phys. Lett.* **72**, 410–411 (1998).
8. P. I. Hsu, R. Bhattacharya, H. Gleskova, M. Huang, Z. Xi, Z. Suo, S. Wagner, and J. C. Sturm, "Thin-film transistor circuits on large-area spherical surfaces," *Appl. Phys. Lett.* **81**, 1723–1725 (2002).
9. M. Berggren, A. Dodabalapur, R. E. Slusher, and Z. Bao, "Light amplification in organic thin films using cascade energy transfer," *Nature (London)* **389**, 466–469 (1997).
10. G. Ramos-Ortiz, C. Spiegelberg, N. Peyghambarian, and B. Kippelen, "Temperature dependence of the threshold for laser emission in polymer microlasers," *Appl. Phys. Lett.* **77**, 2783–2785 (2000).
11. V. G. Kozlov, V. Bulovic, and S. R. Forrest, "Temperature independent performance of organic semiconductor lasers," *Appl. Phys. Lett.* **71**, 2575–2577 (1997).
12. S. Riechel, U. Lemmer, J. Feldmann, S. Berleb, A. G. Mückl, W. Brütting, A. Gombert, and V. Wittwer, "Very compact tunable solid-state laser utilizing a thin-film organic semiconductor," *Opt. Lett.* **26**, 593–595 (2001).
13. M. Maeda, Y. Oki, and K. Imamura, "Ultrashort pulse generation from an integrated single-chip dye laser," *IEEE J. Quantum Electron.* **33**, 2146–2149 (1997).
14. H. Finkelmann, S. T. Kim, A. Munoz, P. Palfy-Muhoray, and B. Taheri, "Tunable mirrorless lasing in cholesteric liquid crystalline elastomers," *Adv. Mater.* **13**, 1069–1072 (2001).
15. A. Dodabalapur, M. Berggren, R. E. Slusher, Z. Bao, A. Timko, P. Schiortino, E. Laskowski, H. E. Katz, and O. Nalamasu, "Resonators and materials for organic lasers based on energy transfer," *IEEE J. Sel. Top. Quantum Electron.* **4**, 67–74 (1998).
16. V. G. Kozlov, G. Parthasarathy, P. E. Burrows, V. B. Khalfin, J. Wang, S. Y. Chou, and S. R. Forrest, "Structures for organic diode lasers and optical properties of organic semiconductors under intense optical and electrical excitations," *IEEE J. Quantum Electron.* **36**, 18–26 (2000).
17. Y. Oki, K. Aso, D. Zuo, N. J. Vasa, and M. Maeda, "Wide-wavelength-range operation of a distributed-feedback dye laser with a plastic waveguide," *Jpn. J. Appl. Phys.* **41**, 6370–6374 (2002).
18. J. Carroll, J. Whiteaway, and D. Plumb, *Distributed Feedback Semiconductor Lasers* (Institution of Electrical Engineers, Stevenage, UK, 1998).
19. C. Bauer, H. Giessen, B. Schnabel, E. B. Kley, C. Schmitt, U. Scherf, and R. F. Mahrt, "A surface-emitting circular grating polymer laser," *Adv. Mater.* **13**, 1161–1164 (2001).
20. T. Kavc, G. Langer, P. Polt, K. Reichmann, and W. Kern, "Formation of images and surface relief gratings in photosensitive polymers containing SCN groups," *Macromol. Chem. Phys.* **203**, 1099–1105 (2002).
21. G. Langer, T. Kavc, W. Kern, G. Kranzelbinder, and E. Toussaere, "Refractive index changes in polymers induced by deep UV irradiation and subsequent gas phase modification," *Macromol. Chem. Phys.* **202**, 3459–3467 (2001).
22. G. Kranzelbinder, E. Toussaere, J. Zyss, T. Kavc, G. Langer, and W. Kern, "Organic surface emitting laser based on a deep-ultraviolet photopolymer containing thiocyanate groups," *Appl. Phys. Lett.* **82**, 2203–2205 (2003).
23. T. Kavc, G. Langer, W. Kern, G. Kranzelbinder, E. Toussaere, G. A. Turnbull, I. D. W. Samuel, K. F. Iskra, T. Neger, and A. Pogantsch, "Index and relief gratings in polymer films for organic distributed feedback lasers," *Chem. Mater.* **14**, 4178–4185 (2002).
24. G. Langer, A. Pogantsch, K. F. Iskra, T. Neger, and W. Kern, "Lasing action in optically written two-dimensional DFB gratings," *Synth. Met.* **137**, 997–998 (2003).
25. A. Donval, E. Toussaere, S. Brasselet, and J. Zyss, "Comparative assessment of electrical, photoassisted and all optical in-plane poling of polymer based electrooptic modulators," *Opt. Mater.* **12**, 215–219 (1999).
26. D. Wright, E. Brassclet, J. Zyss, G. Langer, A. Pogantsch, K. F. Iskra, T. Neger, and W. Kern, "All-optical tunability of holographically multiplexed organic distributed feedback lasers," *Opt. Express* **12**, 325–330 (2004), <http://www.opticsexpress.com>.